J Mater Sci (2011) 46:774–780
DOI 10.1007/s10853-010-4813-9

Optical and electrical properties of aluminum-doped zinc oxide nanoparticles

Yulong Zhang · Ye Yang · Junhua Zhao · Ruiqin Tan · Weiyan Wang · Ping Cui · Weijie Song

Received: 6 May 2010 / Accepted: 30 July 2010 / Published online: 12 August 2010

Abstract Aluminum-doped zinc oxide nanopowders were prepared using a surfactant assisted complex sol–gel method, and were characterized using inductively coupled plasma, X-ray diffraction, scanning electron microscopy/energy dispersive X-ray spectroscopy, X-ray photoelectron spectroscopy, and UV–Vis spectroscopy. Al was effectively doped into the ZnO matrix with concentrations up to 6.00 atomic ratio percents (at.%). X-ray diffraction results revealed that all of the nanoparticles had a pure hexagonal wurtzite structure free of any impurities when annealing temperature was below 1273 K. The optical band gap of the nanopowders, which was affected by the Al-doping concentration, reached a maximum of 3.43 eV when ZnO was doped with 4.00 at.% Al. The effect of post-annealing temperature and vacuum conditions on the resistivities of the Al-doped ZnO nanoparticles was also investigated. And the lowest volume resistivity (1.2 Ω cm) was achieved by annealing the Al-doped ZnO nanoparticles in a vacuum at 1173 K for 2 h.

Y. Zhang · Y. Yang · J. Zhao · W. Wang · P. Cui · W. Song (✉)
Ningbo Institute of Material Technology and Engineering, Chinese Academy of Sciences, No. 519 Zhuangshi Road, Zhenhai District, Ningbo 315201, People's Republic of China
e-mail: weijiesong@nimte.ac.cn

R. Tan
School of Information Science and Engineering, Ningbo University, No. 818 Fenghua Road, Jiangbei District, Ningbo 315211, People's Republic of China

Introduction

Nano-sized zinc oxide (ZnO) powders doped with different ions have improved electrical, optical, and catalytic properties, making them ideal for use in various technological applications [1–10]. Among these, aluminum-doped ZnO (AZO) nanopowders are both conductive and transparent in the visible region and thus can be utilized in transparent conductive pastes [6, 11–14]. Various methods have been reported for preparing AZO nanopowders including sol–gel [1, 4, 14], spray pyrolysis [6], precipitation [10, 15], and hydrothermal processes [16, 17]. The sol–gel process had attracted considerable attention because of its flexibility in fine tailoring particle properties and was easiest to achieve the Al-doped nanopowders [1, 18, 19]. Kim and Tai [20] prepared an 1 atomic ratio percent (at.%) Al-doped ZnO thin films using the sol–gel process and obtained crystal sizes ranging from 13 to 29 nm with annealing temperatures between 773 and 973 K. Serier et al. [1] synthesized AZO nanopowders via the Pechini process with a doping concentration varying from 1.00 to 4.00 mol%, and observed an enhanced infrared absorption properties for the doped samples annealing at 1200 °C. Simultaneously, the optical and electrical properties of AZO nanopowders can be easily tailored by changing the preparation parameters. Kadam et al. [21] studied the optical band gap changes in Al-doped ZnO nanocrystals as a result of Al-doping and the related change in grain size. Lotus et al. investigated the band gap and conductivity of Al-doped ZnO nanofibers. Al-doped ZnO nanofibers exhibited lower band gap energies than did the undoped ZnO nanofibers. And it was found that as the aluminum content (Al/(Al + Zn)) increased from 1.70 to 3.20 at.%, the band gap energy increased, resulting in lower conductivity [2]. Cheng et al. [3] also studied the conductivity of Al-doped ZnO ceramics

with doping concentration varying from 1.00 to 4.00 at.% and obtained a conductivity of 7.5×10^{-4} S/cm with a doping content of 2 at.%. Verma et al. [4] investigated polycrystalline Al-doped ZnO thin film using the sol–gel method and obtained a resistivity of 0.5 Ω cm with a doping content of 3 at.%, and the films had exhibited excellent transmittance (90%) in the 400–1100 nm wavelength range. Thu and Maenosono [22] synthesized a high-quality Al-doped ZnO nanoink by a thermal decomposition method with a good dispersibility. An optical transparent AZO film was fabricated using the nanoink by spin casting, followed by annealing. The resulting AZO thin film resistivity was 5×10^{-3} Ω cm. Though many works had been focused on the preparation of AZO nanoparticles, a systematic investigation on the grain size, optical and electrical properties of the AZO nanoparticles as well as the effect of the post-treatments of the AZO powders on the their resistivity was still lacking. In the first part of this work, AZO nanopowders with different doping concentrations were synthesized using the surfactant assisted complex sol–gel method. The microstructures and optical property were systematically characterized. And then the AZO nanopowders were subjected to various post-annealing treatments. Finally, the resistivities of AZO nanopowders after applying different treatments were summarized.

Experiments

Powder preparation and post-treatments

The AZO nanopowders were synthesized from $Zn(NO_3)_2 \cdot 6H_2O$, $Al(NO_3)_3 \cdot 9H_2O$, citric acid (CA), and polyethylene glycol (PEG) using the surfactant assisted complex sol–gel method [23]. The mixed transparent solution containing 0.03 mol $Zn(NO_3)_2 \cdot 6H_2O$ and the $Al(NO_3)_3 \cdot 9H_2O$ with various contents (Al/(Al + Zn) = 0.00, 2.00, 4.00, 6.00 at.%) was dissolved in 50 mL de-ionic water and was dripped into the CA (0.045 mol) and PEG 2000 (0.003 mol) solution (50 mL). The total volume of this solution was 100 mL. The pH of formed solution was adjusted to 1 using ammonia (17 wt%). The solution was then immersed in a 353 K water bath with stirring for 4 h and aged at room temperature for another 4 h. The transparent solution was gelled at 358 K and was immediately put into a vacuum until it turned into xerol, which was then sintered in a furnace at 773 K for 4 h in air. The AZO nanopowders were milled in an agate mortar and were further annealed at 773, 1173, and 1273 K for 2 h in air. The obtained nanopowders were pressed into coin-shaped samples at 300 MPa to measure the resistivity. In order to study the effect of post-treatment conditions on the materials, the nanopowders were annealed in a high vacuum furnace at 773 and 1173 K for 2 h in vacuum (10^{-4} Pa) to remove the adsorbed oxygen on the surface.

Powder characterization

A Bruker AXS D8 Advance diffractometer was used with Cu Kα radiation at a power of 1.6 kW to take X-ray diffraction (XRD) measurements. The diffraction patterns were calibrated using the standard corundum spectra. The instrument broadening (the FWHM curve of standard corundum) was subtracted before estimating the grain size using the Scherrer equation. The inductively coupled plasma (ICP) analysis was conducted using a Perkin-Elmer Optima 2100 with 22 kW continuous electric powers with a nominal frequency of 1 MHz. The powder (0.1 g) was dissolved into HNO_3 solution (HNO_3:H_2O = 1:1 volume ratio), and then was set to be 100 mL using de-ionic water for analysis. The chemical composition and chemical states were characterized using X-ray photoelectron spectroscopy (XPS) (Ultra^{DLD}, Kratos, UK) with a monochromatic Al Kα source and pass energy of 10 eV. The morphology was recorded using a Hitachi S-4800 field emission scanning electron microscope (FESEM). The small area composition analysis was performed using energy dispersive X-ray spectroscopy (EDX) on a Hitachi S-4800 SEM/EDX (Japan). The obtained nanopowders were dispersed in cyclohexane under ultrasonic condition (600 W) with a concentration of 5 mg/mL for UV–Vis analysis. The optical transmission spectra at various concentrations were recorded using an ultraviolet–visible–near infrared (UV–visible–NIR) spectrometer (Perkin Elmer Lambda 950) with a wavelength range of 200–800 nm at room temperature. The resistivities of all ZnO-based nanopowders were measured on Keithley 237 using the method described in Ref. [24].

Results and discussion

Structures and composition of AZO nanopowders

Figure 1 shows the XRD results for the pristine and Al-doped ZnO nanopowders. All diffraction peaks could be perfectly indexed to the wurtzite ZnO reported in JCPDS (036-1451) [25]. This result suggested that the nanopowders had a pure hexagonal wurtzite structure with well-developed crystallinity. The (002) diffraction peak position of the XRD signals detected from the AZO nanopowders was revised taking into consideration a shift of 0.40° towards a higher angle than that of the pristine ZnO. This was due to the lattice shrinkage caused by the Al^{3+} (radius is 0.53 Å) replacing the Zn^{2+} (radius is 0.74 Å) [21, 26, 27]. Figure 2 shows the full width at half maximum

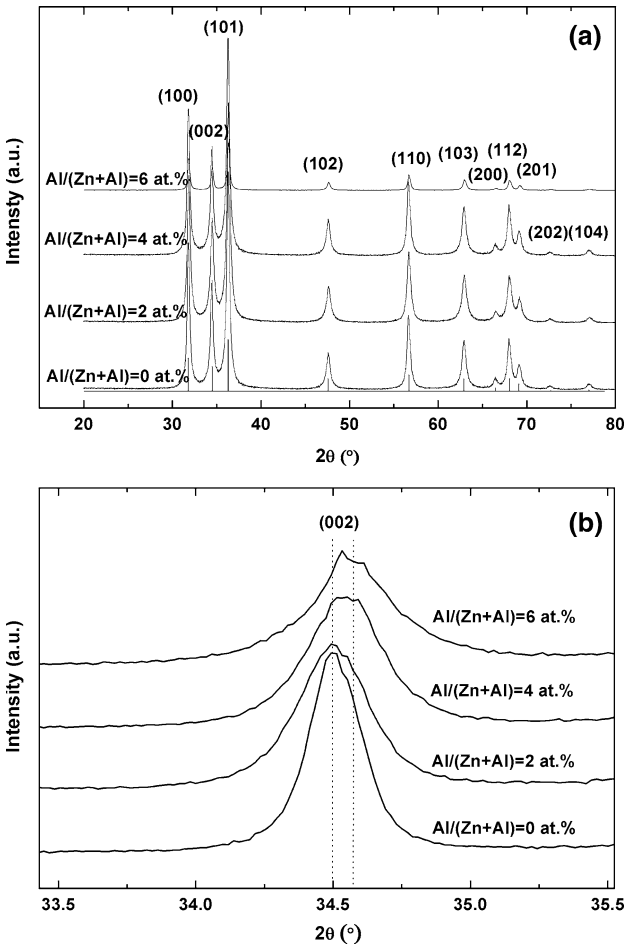

Fig. 1 **a** XRD patterns of the Al-doped ZnO nanoparticles at different doping concentrations from 0.00 to 6.00 at.%; **b** (002) peak of Al-doped ZnO nanoparticles (Al/(Al + Zn) = 0.00, 2.00, 4.00, 6.00 at.%)

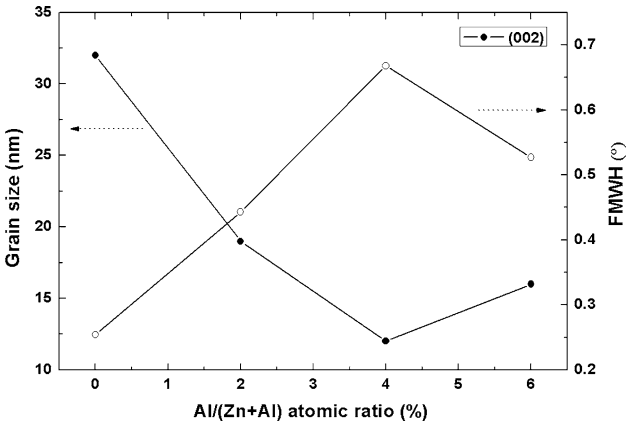

Fig. 2 Full width at half maximum of the (002) XRD peaks (*circle*) and the calculated average grain size (*black dot*) of the Al-doped ZnO nanoparticles as a function of the Al-doping concentration

(FWHM) value of (002) diffraction peaks and corresponding average grain size calculated from the Scherrer equation [28] as a function of the doping concentration. The average grain size decreased from 34 to 12 nm when the aluminum doping concentration increased from 0.00 to 4.00 at.%. This was due to the decreased sintering rate that occurred when the Al atoms were incorporated into the ZnO lattice during the sol–gel process [29]. Figure 3 shows the SEM results for the powders synthesized under the sol–gel conditions. It was noted that with increasing Al, the average particle size of the sphere-shaped AZO was reduced. This was in good agreement with the XRD results.

The nominal doping concentration and the doping concentration measured with ICP are listed in Table 1. The Al contents of the nanopowders were quite close to that of the original materials, indicating that Al was mostly incorporated into the ZnO matrix during this process. Figure 4 shows the EDX results indicating that the Al content was 2.00 at.% in the original materials. As shown in Fig. 4, the Al content of the nanopowders was ca. 2.50 at.%. Thus, Al content in the nanopowders was greater than that in the original materials. The XPS spectrum of Al-doped ZnO (4.00 at.%) shown in Fig. 5 suggested that Al was presented on the surface of the samples. No Al^0 was observed in the samples. The high-resolution XPS spectrum of the inserted Al 2p showed that the peak was centered at 74.7 eV, indicating the presence of Al^{3+} on the surface of the AZO nanoparticles [1, 30].

Optical properties

Figure 6 shows the optical transmission spectra of the AZO nanopowder suspension. The AZO nanopowders revealed a consistent blue-shift at the doping concentration from 2.00 to 4.00 at.% and a red-shift at 6.00 at.% compared with that of the 4.00 at.% Al-doped ZnO. Figure 7 summarizes the band gap calculated from the transmission data. The band gap of Al-doped ZnO increased with the Al-doping concentrations from 2.00 to 4.00 at.% compared with that of the pristine ZnO, achieving a maximum value of 3.43 eV at 4.00 at.%, and then decreased at 6.00 at.%. The question to be resolved at this point was whether the blue-shift could be attributed to a Moss–Burstein type shift in the AZO nanopowders or whether it was partially due to the quantum confinement effect caused by the incorporation of Al^{3+}. According to quantum confinement theory, the energy band gap of a semiconductor depends on the crystal size, and its value will increase as the crystal size decreases [31, 32]. Viswanatha et al. [33] developed a realistic and accurate tight binding (TB) scheme to explain the blue-shift and correlate the absorption edge with the size of the nanocrystal. According to Viswanatha et al.'s model calculation, the blue-shift caused by the quantum confinement effect was only 0.03 eV when the particle size

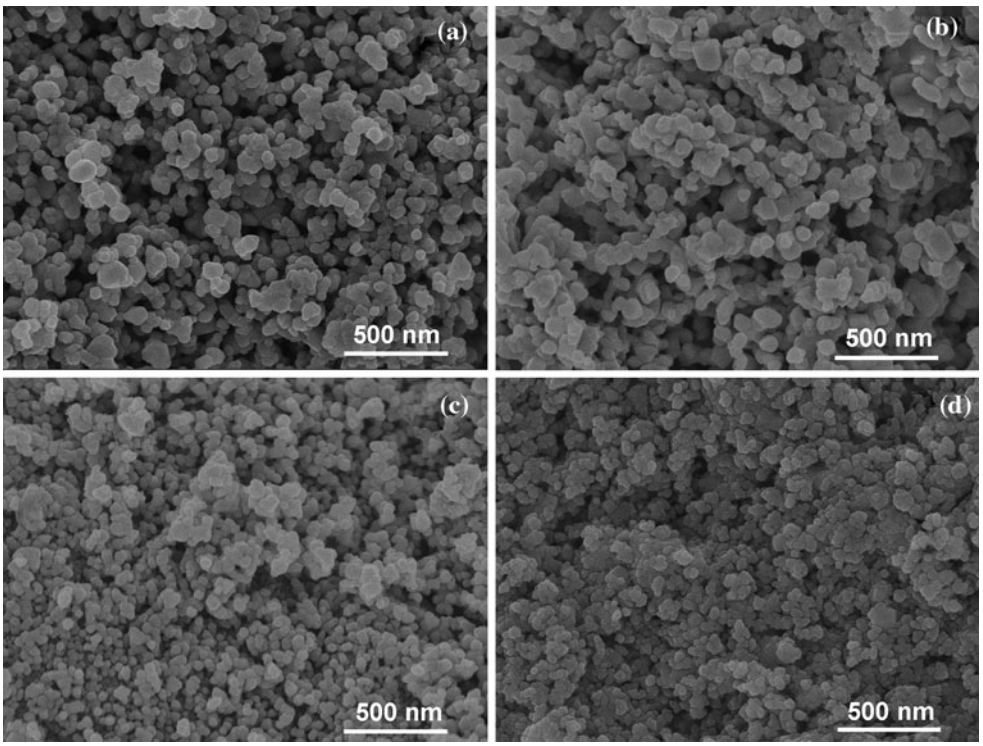

Fig. 3 SEM images of the Al-doped ZnO nanoparticles **a** Al/(Zn + Al) = 0.00 at.%, **b** Al/(Zn + Al) = 2.00 at.%, **c** Al/(Zn + Al) = 4.00 at.%, **d** Al/(Zn + Al) = 6.00 at.%

Table 1 Procedure ratios added in the original materials and results of the ICP analysis on the Al-doped ZnO nanoparticles

Model	Al contents in the starting materials (%)	Al contents by ICP (%)
①	Al/(Zn + Al) = 0.00 at.%	Al/(Zn + Al) = 0.02 at.%
②	Al/(Zn + Al) = 2.00 at.%	Al/(Zn + Al) = 1.95 at.%
③	Al/(Zn + Al) = 4.00 at.%	Al/(Zn + Al) = 3.54 at.%
④	Al/(Zn + Al) = 6.00 at.%	Al/(Zn + Al) = 5.34 at.%

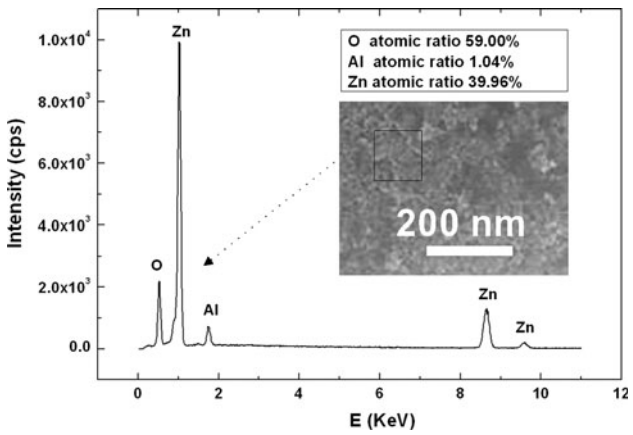

Fig. 4 EDX spectrum of the Al-doped ZnO nanoparticles at Al/(Zn + Al) = 2.00 at.%

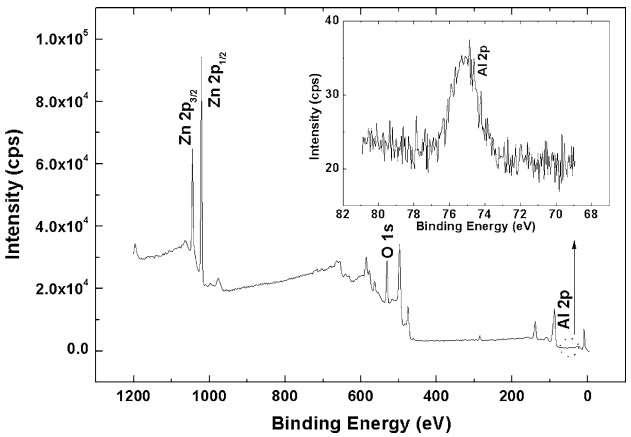

Fig. 5 XPS wide scan spectra of the Al-doped ZnO nanoparticles (4.00 at.%) with Al 2p spectrum inserted

decreased from 34 to 12 nm, while the optical band breadth in our experiment was 0.12 eV (3.43–3.31 eV). Since this high value did not fit with the particle size decreased as calculated with the model of Viswanatha et al., and thus could not be explained by a confinement effect. However, our results suggested that the Al-doping affected the band gap, in what we believed to be a Burstein type shift due to Al-doping proved by various previous studies [34–36].

Interestingly, the band gap variation was more pronounced in the case of high Al-doping nanopowders (above 4.00 at.%) since the band gap did not increase

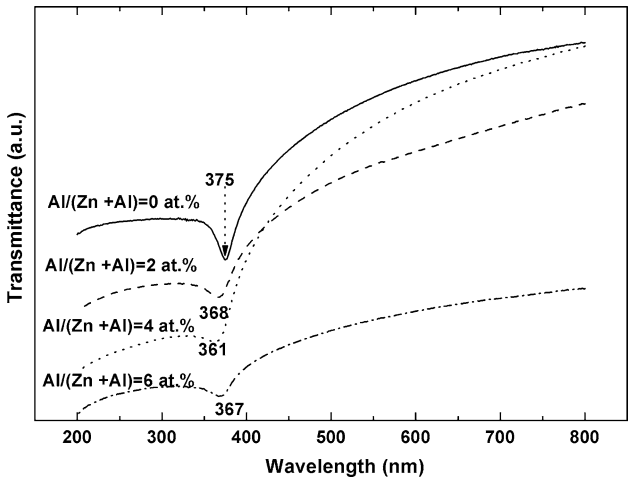

Fig. 6 UV–Vis spectra of the Al-doped ZnO nanoparticles at different doping concentrations

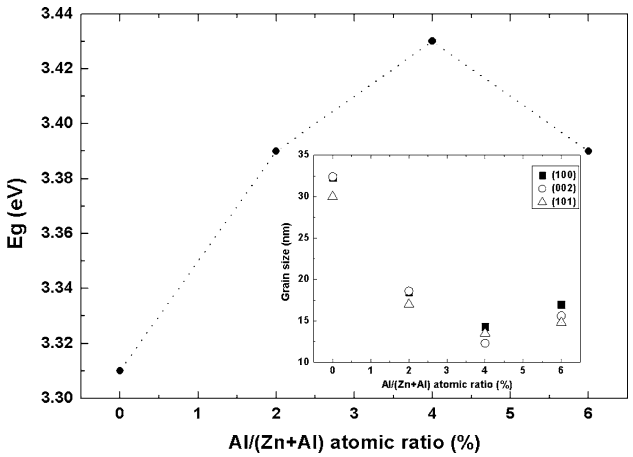

Fig. 7 Optical band gaps of the Al-doped ZnO nanoparticles as a function of the Al-doping concentration with average grain size of the Al-doped particles inserted

monotonically with the dopant concentrations. It was noted that the band gap variation was quite similar to that of the Al-doped ZnO thin film reported by Park. An initial increase in the band gap was observed in our experiments, followed by a decrease [24]. The band gap, E_g, was expected to increase with the Al contents, since the band gap of Al_2O_3 (bulk band gap = 6.4 eV) was greater than that of ZnO (bulk band gap = 3.30 eV) [37]. According to the Burstein–Moss effect, the broadening of the optical band gap is:

$$\Delta E_g = \left(\frac{\hbar^2}{2m^*_{cv}}\right)(3\pi^2 n)^{\frac{2}{3}} \quad (1)$$

where ΔE_g is the shift of the doped semiconductor with respect to the pristine semiconductor, m^*_{cv} is the reduced effective mass, $\hbar$ is Plank constant, n is the free carrier concentration, and π is a constant. According to this equation, the band gap should increase with carrier concentration. The decrease of E_g also observed by Park et al. [26] at a concentration of 6.00 at.% was in accordance with the decrease of n_e. The Al-doping mechanism could be described as [26]:

$$Al_2O_3 + ZnO \rightarrow Zn_{Zn} + 2Al^{\bullet}_{Zn} + 3O^{\times}_{o} + \frac{1}{2}O_2(g) + 2e^- \quad (2)$$

$$O^{\times}_{o} + 2e^- \rightarrow O^{2-} \quad (3)$$

The electronic concentration in the AZO gradually decreased as O^{2-} was increased, as shown in the formula (3). Park et al. [38] experiment on AZO films produced by pulse laser deposition yielded a similar result. Thus, as more Zn^{2+} was replaced by Al^{3+}, the decrease in carrier concentration could be attributed to excessive oxygen. Thus, on the one hand, the band gap of Al-doping at 6.00 at.% decreased with the carrier concentration because electrons were depleted by the excessive oxygen produced as Al replaced Zn. On the other hand, the decrease of ΔE_g broadening on the Al/(Zn + Al) = 6.00 at.% sample might be related to the amorphous alumina, which indicated a solid solubility limit of less than 4.00 at.% in the AZO nanopowders prepared at 773 K.

Electrical properties

The high resistivities of Al-doped ZnO nanopowders made it ineffective as a conductive material because of electron scattering and the trap effects of adsorbed oxygen on the grain boundaries. Thus, post-treatments were applied to reduce the resistivity of the Al-doped ZnO nanopowders. As reported in other studies, the number of grain boundaries could be reduced by increasing the annealing temperature. In addition, Zn is replaced by Al. Here, the effect of annealing temperature on powder resistivity was investigated. Figure 8a–c illustrated the relationship between resistivity and the Al-doping concentration for the Al-doped ZnO nanopowders annealed in air at 773, 1173, and 1273 K, respectively. The XRD pattern of the sample (2 at.%) sintered at 1273 K was also inserted in, signed as Fig. 8d. In our experiments, the samples were sintered in air at 773, 1173, and 1273 K for 6 h. Powder resistivity decreased from ca. 10^8 Ω cm (773 K) to ca. $10^3/10^4$ Ω cm (1273 K) for both the pristine ZnO and the Al-doped ZnO nanoparticles (Al/(Al + Zn) = 2.00, 4.00, 6.00 at.%). There were two processes at work here. First, grain growth occurred at higher annealing temperatures [23]. Second, increased Al effectively reduced AZO powder resistivity. The minimum value we achieved was an Al/(Zn + Al) atomic ratio of 4.00 at.% at 1273 K, with some increase at 6.00 at.%. Similar results were obtained for the AZO thin

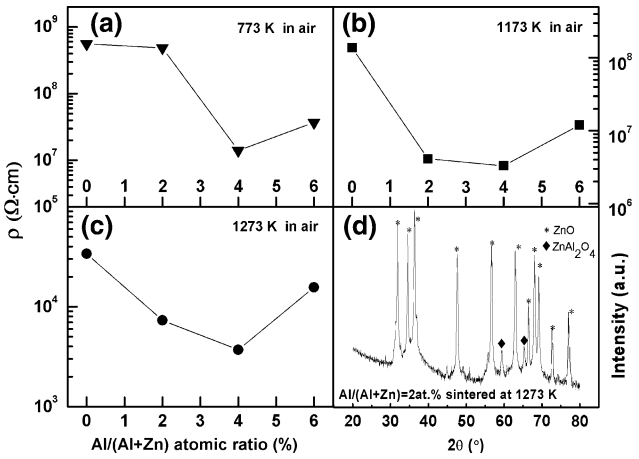

Fig. 8 Resistivity of the Al-doped ZnO nanoparticles annealed in air at different temperatures: (**a**) 773 K, (**b**) 1173 K, (**c**) 1273 K, (**d**) XRD pattern of the Al-doped ZnO nanoparticles annealed in air at 1273 K

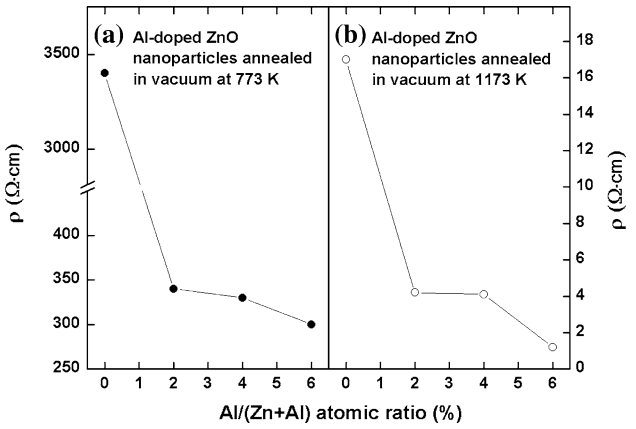

Fig. 9 Resistivity of the Al-doped ZnO nanoparticles annealed at different temperatures in a vacuum: (**a**) $T = 773$ K (*black dot*), (**b**) $T = 1173$ K (*circle*)

films [39, 40]. Although the resistivity of these Al-doped ZnO samples decreased drastically from 10^8 to 10^3 Ω cm by increasing the post-treatment temperatures, it did still not meet the requirements for use as a conductive material. The adsorbed oxygen on the surface of AZO nanoparticles acted as an electron "trap" to increase the resistivities of the AZO powders [37, 41]. Therefore, post-annealing experiments had to be conducted to remove the adsorbed oxygen on the surface of the AZO nanoparticles in order to reduce the resistivity of the AZO nanopowders. Thus, the Al-doped samples were vacuum annealed in the next part.

Figure 9a and b shows the relationship between the resistivity and doping contents of the AZO nanoparticles after post-annealing in a vacuum (10^{-4} Pa). Since the $ZnAl_2O_4$ spinel phase occurred at 1273 K, the annealing temperatures were chose at 773 and 1173 K here. The resistivities of the pristine ZnO nanopowders decreased by more than 5 orders of magnitude (10^8–10^3 Ω cm) after annealing in a vacuum at 773 K and more than 4 orders of magnitude (10^7–10^3 Ω cm) after annealing in a vacuum at 1173 K compared with the results of the pristine ZnO annealed in air as shown in Fig. 8. And the resistivity reduction of the 2.00 at.% Al-doping ZnO nanopowders annealed in vacuum was similar to that of the 4.00 and 6.00 at.% Al-doping ZnO nanopowders annealed in vacuum both at 773 and at 1173 K, which decreased more than 7 orders of magnitude (10^7–10^0 Ω cm) compared with those AZO (Al/(Al + Zn) = 2.00, 4.00, 6.00 at.%) nanopowders annealed in air (Fig. 8a, b). This might be due to the existence of non-conductive amorphous Al_2O_3 in the ZnO nanopowders with high Al-doping concentration. The lowest resistivity of 1.2 Ω cm was obtained when the AZO nanopowders (Al/(Al + Zn) = 6.00 at.%) was sintered in a vacuum at 1173 K shown in Fig. 9b.

Conclusion

In summary, The AZO nanopowders with different Al-doping concentrations have been successfully prepared. And the effects of Al-doping on the structural, optical, and electrical properties of the ZnO powders were investigated. The AZO powders had a pure wurtzite structure. The optical band gap of the pristine ZnO nanopowders was similar to that of single crystal ZnO (3.3 eV), and the optical band gap of Al-doped ZnO nanopowders was larger than that of the pristine ZnO nanopowders. And the maximum was 3.43 eV when the Al-doping content was 4.00 at.%. After post-annealing treatments in air, the AZO nanopowders' resistivity decreased with increasing annealing temperatures up to 1273 K. The samples annealed in a vacuum at 773 and 1173 K displayed monotonically decreasing resistivity as the Al-doping concentration increased. The lowest volume resistivity was 1.2 Ω cm (Al/(Al + Zn) = 6.00 at.%), obtained when the AZO nanopowders was sintered in vacuum at 1173 K.

Acknowledgements Financial supports from the Hundred Talents Program, the Solar Action Program, and the Innovative Research International Partnership Program of Chinese Academy of Sciences, the Ningbo Innovative Research Team Program, and the Zhejiang Natural Science Foundation (Y407364) are highly appreciated.

References

1. Serier H, Gaudon M, Ménétrier M (2009) Solid State Sci 11:1192. doi:10.1016/j.solidstatesciences.2009.03.007
2. Lotus AF, Kang YC, Walker JI, Ramsier RD, Chase GG (2010) Mater Sci Eng B 166:61. doi:10.1016/j.mseb.2009.10.001
3. Cheng H, Xu XJ, Hng HH, Ma J (2009) Ceram Int 35:3067. doi:10.1016/j.ceramint.2009.04.010
4. Verma A, Khan F, Kar D, Chakravarty BC, Singh SN, Husain M (2010) Thin Solid Films 518:2649. doi:10.1016/j.tsf.2009.08.010

5. Pál E, Dékány I (2008) Colloids Surf A 318:141. doi:10.1016/j.colsurfa.2007.12.028
6. Ogi T, Hidayat D, Iskandar F, Purwanto A, Okuyama K (2009) Adv Powder Technol 20:203. doi:10.1016/j.apt.2008.09.002
7. Ahn BD, Kang HS, Kim JH, Kim GH, Chang HW, Lee SY (2006) J Appl Phys 100:093701(1–6). doi:10.1063/1.2364041
8. Brayner R, Ferrarilliou R, Brivos N, Djediat S, Benedetti MF, Fiévet F (2006) Nano Lett 6:866
9. Kamat PV, Patrick B (1992) J Phys Chem 96:6829
10. Du SF, Tian YJ, Liu HD, Liu J, Chen YF (2006) J Am Ceram Soc 89:2440. doi:10.1111/j.1551-2916.2006.01093.x
11. Hammarberg E, Schwab AP, Feldmann C (2009) J Colloid Interface Sci 334:29. doi:10.1016/j.jcis.2009.03.010
12. Ismail B, Abaab M, Rezig B (2001) Thin Solid Films 383:92
13. Lü N, Lü XD, Jin X, Lü CL (2007) Polym Int 56:138. doi:10.1002/pi.2126
14. Ji LW, Shih WS, Fang TH, Wu CZ, Peng SM, Meen TH (2010) J Mater Sci 45:3266. doi:10.1007/s10853-010-4336-4
15. Chen XG, He YQ, Zhang Q, Li LJ, Hu DH, Yin T (2010) J Mater Sci 45:953. doi:10.1007/s10853-009-4025-3
16. Zhang H, Yang D, Li SZ, Ma XY, Ji YJ, Xu J, Que DL (2005) Mater Lett 59:1696. doi:10.1016/j.matlet.2005.01.056
17. Zhang WH, Zhang WD, Zhou JF (2010) J Mater Sci 45:209. doi:10.1007/s10853-009-3920-y
18. Tsubota T, Ohtaki M, Eguchi K, Arai H (1997) J Mater Chem 7:85
19. Yoon MH, Lee SH, Park HL, Kim HK, Jang MS (2002) J Mater Sci Lett 21:1703
20. Kim YS, Tai WP (2007) Appl Surf Sci 253:4911. doi:10.1016/j.apsusc.2006.10.068
21. Kadam P, Agashe C, Mahamuni S (2008) J Appl Phys 104:103501. doi:10.1063/1.3020527
22. Thu TV, Maenosono S (2010) J Appl Phys 107:014308. doi:10.1063/1.3273501
23. Zhang YL, Yang Y, Zhao JH, Tan RQ, Cui P, Song WJ (2009) J Sol-Gel Sci Technol 51:198. doi:10.1007/s10971-009-1959-5
24. Wang RP, Sleight AW (1996) Chem Mater 8:433
25. JCPDS, "Powder diffraction file of inorganic phases, Joint Committee on Powder Diffraction Standards," Swarthmore, PA, Powder Diffraction File No. 36-1451 (1997)
26. Park KC, Ma DY, Kim KH (1997) Thin Solid Films 305:201
27. Navale SC, Ravi V, Mulla IS, Gosavi SW, Kulkarni SK (2007) Sens Actuators B 126:382. doi:10.1016/j.snb.2007.03.019
28. Chen M, Wang X, Yu YH, Pei ZL, Bai XD, Sun C, Huang RF, Wen LS (2000) Appl Surf Sci 158:134
29. Mazaheri M, Zahedi AM, Sadrnezhaad SK (2008) J Am Ceram Soc 91:56. doi:10.1111/j.1551-2916.2007.02029.x
30. Brehm JU, Winterer M, Hahn H (2001) J Appl Phys 100:064311(1–9). doi:10.1063/1.2349430
31. Wang YG, Lau SP, Lee HW, Yu SF, Tay BK, Zhang XH, Hng HH (2004) J Appl Phys 94:354. doi:10.1063/1.1577819
32. Srinivasan G, Rajendra Kumar RT, Kumar J (2007) Opt Mater 30:314. doi:10.1016/j.optmat.2006.11.075
33. Viswanatha R, Sapra S, Satpati B, Satyam PV, Dev BN, Sarma DD (2004) J Mater Chem 14:661. doi:10.1039/b310404d
34. Jeong C, Kim HS, Chang DR, Kamisako K (2008) Jpn J Appl Phys 47:5656. doi:10.1143/JJAP.47.5656
35. Viswanatha R, Sapra S, Gupta SS, Satpati B, Satyam PV, Dev BN, Sarma DD (2004) J Phys Chem B 108:6303
36. Shan FK, Yu YS (2004) J Eur Ceram Soc 24:1869. doi:10.1016/S0955-2219(03)00490-4
37. Nguyen NV, Kirillov Oleg A, Jiang W, Wang WY, Suehle JS, Ye PD, Xuan Y, Goel N, Choi KW, Tsai W, Sayan S (2008) J Appl Phys 93:082105. doi:10.1063/1.2976676
38. Park SM, Ikegami T, Ebaharai K (2005) Jpn J Appl Phys 44:8027. doi:10.1143/JJAP.44.8027
39. Minami T, Satio H, Nanto H, Takata S (1985) Jpn J Appl Phys 24:L781
40. Bai SN, Tseng TY (2006) Thin Solid Films 515:872. doi:10.1016/j.tsf.2006.07.048
41. Tahar RBH, Tahar NBH (2002) J Appl Phys 92:4498. doi:10.1063/1.1509083